

On the Modeling of Wall Surface Pressure Spectra for Trailing Edge Noise Prediction

Carolin Kissner*, Sébastien Guérin †
German Aerospace Center (DLR), Berlin, 10623, Germany

Stefano Bianchi ‡, Thomas Nodé-Langlois §
Airbus Commercial Aircraft, Toulouse, 31060, France

Broadband noise is a significant source for open rotors and Ultra High Bypass Ratio fans. The analytical description of the leading edge noise component is typically linked to the upwash velocity autospectrum of the impinging turbulence, and the modeling of the trailing edge component due to the interaction of the boundary layer turbulence with the trailing edge relies on the surface pressure autospectrum near the trailing edge. But while there is some consensus on describing transverse velocity frequency spectra for leading edge noise, there are a plethora of different models of varying complexity to describe wall surface pressure autospectra. Choosing an appropriate model to apply in the framework of fast and robust acoustic prediction tools is therefore no easy task. This paper aims to apply different models for predicting the surface pressure spectrum near the trailing edge of an airfoil. Experimental data for two airfoils at realistic flight Mach and Reynolds numbers were studied and different RANS-informed empirical models as well as the Stalnov TNO model were investigated regarding their ability to capture experimental trends.

I. Nomenclature

C_D	=	drag coefficient
c	=	chord length, m
c_0	=	speed of sound, m/s
f	=	frequency, Hz
H	=	boundary layer shape factor, $\frac{\delta^*}{\theta}$
k_1	=	streamwise wavenumber, $1/m$
k_3	=	spanwise wavenumber, $1/m$
k_e	=	normalized wavenumber of main energy bearing eddies, $\frac{\sqrt{\pi}}{\Lambda(x_2)} \frac{\Gamma(5/6)}{\Gamma(1/3)}$
k_t	=	kinetic turbulent energy, m^2/s^2
$L_{2,22}$	=	correlation length scale perpendicular to blade surface, m
Ma	=	Mach number, $\frac{U_0}{c_0}$
MS	=	empirical normalized spectrum
p	=	pressure, Pa
p_w	=	wall pressure, Pa
U_0	=	free stream velocity, m/s
U_1	=	mean velocity parallel to the blade surface in a boundary layer, m/s
U_c	=	convective mean velocity, m/s
U_e	=	mean velocity at the edge of the boundary layer, m/s
u_2	=	fluctuating velocity perpendicular to wall surface, m/s
u_τ	=	friction velocity, $\sqrt{\tau_w/\rho_w}$
Re	=	chordwise Reynolds number, $\frac{U_0 c}{\nu}$

*Research Scientist, Institute of Propulsion Technology, Department of Engine Acoustics, carolin.kissner@dlr.de.

†Research Scientist, Institute of Propulsion Technology, Department of Engine Acoustics, sebastien.guerin@dlr.de.

‡Acoustics Engineer, Airbus Commercial Aircraft, Turbomachinery Aeroacoustics, stefano.bianchi@airbus.com.

§Acoustics Engineer, Airbus Commercial Aircraft, Acoustics Methods, thomas.node-langlois@airbus.com.

R_T	=	time-scale ratio, $\left(\frac{\delta}{U_e}\right) / \left(\frac{\nu}{u_\tau^2}\right)$
Re_τ	=	Reynolds number based on wall shear stress, $\frac{u_\tau \delta}{\nu}$
Re_θ	=	Reynolds number based on boundary layer momentum thickness, $\frac{U_e \theta}{\nu}$
SF	=	spectral scaling factor
β_i	=	anisotropy stretching factor with respect to direction i , $\frac{\overline{u_i^2}}{u_1^2}$
β_C	=	Clauser's equilibrium parameter, $\left(\frac{\theta}{\tau_w}\right) \left(\frac{dp}{dx}\right)$
γ	=	coherence
Δ	=	boundary layer thickness ratio, $\frac{\delta}{\delta^*}$
δ	=	boundary layer thickness, m
δ^*	=	boundary layer displacement thickness, m
δ_w	=	wake width, $\delta_w \approx 2\delta$
θ	=	boundary layer momentum thickness, m
Λ	=	integral length scale, m
$\Lambda_{2,22}$	=	turbulent length scale perpendicular to blade surface, m
$\Lambda_{p 3}$	=	spanwise correlation length of pressure, m
Π	=	Cole's wake parameter, $0.8(\beta_C + 0.5)^{0.75}$
ρ	=	density, kg/m^3
ρ_e	=	density at the edge of the boundary layer, kg/m^3
τ_{max}	=	maximum wall shear stress, $\max\left(\mu_w \left(\frac{dU_0}{ds}\right)_w\right)$
τ_w	=	wall shear stress, $\mu_w \left(\frac{dU_0}{ds}\right)_w$
Φ_{pp}	=	power spectral density of wall surface pressure fluctuations, $Pa^2 \cdot s$
ϕ_{22}	=	power spectral density of transverse velocity fluctuations perpendicular to wall surface, m^2/s
ω	=	angular frequency, rad/s
$\tilde{\omega}$	=	Strouhal number

II. Introduction

Broadband noise in Ultra High Bypass Ratio (UHBR) fans and Contra-Rotating Open Rotors (CROR) consists of interaction noise (or leading edge noise) and self-noise, which mainly consists of trailing edge noise. Leading edge noise occurs due to the interaction of turbulence with the leading edge of an airfoil and is characterized by the transverse velocity autospectrum of the impinging turbulence. Most analytical acoustic tools rely on either the von Kármán spectrum or the very similar Liepmann spectrum to model the inflow turbulence. Among other authors, Guérin et al. [1] showed that a satisfactory agreement can be reached when those isotropic turbulence spectra are used to predict rotor-stator-interaction noise. Trailing edge noise is caused by the interaction of boundary layer turbulence with the trailing edge of an airfoil and the critical ingredient for its prediction is the wall surface pressure autospectrum near the trailing edge, as Ayton et al. [2] have also recently discussed in their paper. In contrast to the transverse velocity spectrum associated with leading edge noise, no comparable consensus exists within the scientific community for modeling the wall surface pressure autospectrum associated with trailing edge noise. At this point, developers of fast and robust acoustic prediction tools face a predicament: There are currently many available models for the prediction of wall surface pressure spectra, which can yield vastly different results for the same airfoil as e.g. demonstrated by Nodé-Langlois et al. [3], Hu [4], Lee [5] and many other authors. Since these fast acoustic prediction tools are often applied in the context of multidisciplinary optimization schemes to yield silent future engine designs, the applied models for the prediction of wall pressure spectra near airfoil trailing edges need to be robust. In addition, they need to be capable of reliably reproducing trends under realistic flight conditions.

While numerical methods like stochastic, synthetic turbulence [6–8], large eddy simulation [9–11], or direct numerical simulation [12–15] techniques have also been applied to study trailing edge noise, these models are not attractive for the integration in fast design tools. However, the detailed insights into the flow structures can help to advance analytical methods. Analytical models for predicting the wall surface pressure autospectrum near the trailing edge of an airfoil range from purely empirical to statistical models. Statistical models [16–23] aim to solve a Poisson equation. The right-hand side of this Poisson equation consists of a mean shear term and a turbulence-turbulence

interaction term:

$$\frac{1}{\rho} \left(\frac{\partial}{\partial x_i} \right)^2 p' = -2 \frac{\partial u_j}{\partial x_i} \frac{\partial U_i}{\partial x_j} - \frac{\partial^2}{\partial x_i \partial x_j} (u_i u_j - \overline{u_i u_j}), \quad (1)$$

where p' denotes pressure fluctuations and U_i and u_i respectively denote mean and fluctuating velocities in the i -direction. For realistic flows, the formulation for computing the wall surface pressure spectra involves multi-dimensional integrals, which pose a problem in terms of the numerical complexity and require a specialized integration technique like a Monte Carlo integration scheme. Another approach, which was first suggested by Parchen [24] based on the theory of Blake [25], is to approximate the solution of the Poisson equation. These so-called TNO models [26–29] focus on the mean shear term and rely on some empirical assumptions regarding the local mean convection velocity, the spanwise correlation length scale, and some turbulence characteristics of the boundary layer. The applied simplifications circumvent the need for a more involved integration scheme. Finally, empirical models [4, 5, 30–34] follow a completely different approach and apply a scaling law based on free stream and boundary layer parameters and calibrated to collapse the curve to fit a normalized spectrum. These models are typically derived for experimental data sets in similar flow conditions. A comprehensive comparison of empirical models is given by Lee [5]. Lee also reexamines commonly used data sets, which served as a basis for deriving different empirical formulations. All of these data bases have one commonality: the academic test cases were performed at relatively low speeds, i.e. between Mach numbers of 0.05 to about 0.2. In contrast, Mach numbers (and Reynolds numbers) encountered at flight conditions are significantly higher.

This paper focuses on the application of such methods in an industrial context. Specifically, it investigates which model for predicting wall pressure autospectra near the trailing edge of an airfoil is potentially suitable to be used in conjunction with fast and robust acoustic prediction tools. This study focuses on selected empirical models [4, 5, 32, 33, 35, 36] and the Stalnov TNO model [28], as these models are considered to be simple enough to be integrated into fast acoustic prediction schemes. The authors examine two airfoils, which were tested in the DNW-TWG wind tunnel at realistic flight Mach and Reynolds numbers. Investigated Mach numbers ranged between 0.38 to 0.70 and Reynolds numbers between 0.9 to 4 million. The measured wall pressure autospectra are examined and trends are identified with respect to angles of attack, chordwise position, Mach numbers, and Reynolds numbers. RANS simulations are performed to gain a deeper insight into the flow on the surfaces of the blades. The boundary layer parameters are extracted as they cannot be directly determined from experimental data for this test case.

III. Experimental setup and data processing

In the framework of the CRORTET project, two different two-dimensional (2D) airfoils were tested in the DNW-TWG wind tunnel at different angles of attack, Mach numbers, and Reynolds numbers. Note that the Reynolds number in the DNW-TWG wind tunnel can be changed by varying the ambient pressure. The so-called CROR airfoil was designed by NLR using an inverse aerodynamic design method with the aim of achieving a pressure distribution on a 2D airfoil, which is comparable to the pressure distribution of a CROR front blade section at 87.5% of the blade span at take-off conditions. The Valeo Controlled-Diffusion (CD) airfoil was originally developed as part of an air conditioning unit by Valeo and is more representative of a compressor or fan root airfoil. Both airfoils were equipped with static as well as unsteady pressure sensors along their chords. Near the trailing edge position, multiple unsteady pressure sensors were also distributed in the spanwise direction. Most analyses in this paper focus on the CROR airfoil at its design point at $\text{AoA} = 5^\circ$, $\text{Re} = 4 \text{ Mio.}$, and $\text{Ma} = 0.55$.

To identify trends that are characteristic of trailing edge noise, it was assumed that the wall pressure autospectrum at an Angle of Attack (AoA) of 0° , where the AoA is defined with respect to the chord line, mainly consists of background noise, especially due to the use of a non-anechoic wind tunnel. Therefore, the spectrum at an AoA of 0° was subsequently subtracted from the spectra at higher AoA's. The impact of this post-processing is illustrated in Fig. 1 for the CROR airfoil at a Mach number of 0.55 and a Reynolds number of 4 million. After post-processing and despite the noise pollution up to an AoA of 4° in the low and medium frequency range, a clear pattern emerges: The frequency peak shifts towards lower frequencies for higher AoA's, which tend to feature thicker boundary layers. Simultaneously, the amplitude of the frequency peak increases with increasing AoA's. In general, signal contamination is likely a factor at lower frequencies at all angles of attack. At lower angles of attack, more severe signal contamination can also be observed in the low to mid frequency domain. Also note that the raw signals include tonal peaks related to the blade passing frequency (and harmonics) of the wind tunnel drive and no smoothing/filtering was applied to remove the corresponding peaks.

At a relative chordwise position of 0.98, eight sensors were positioned at different spanwise locations. The coherence

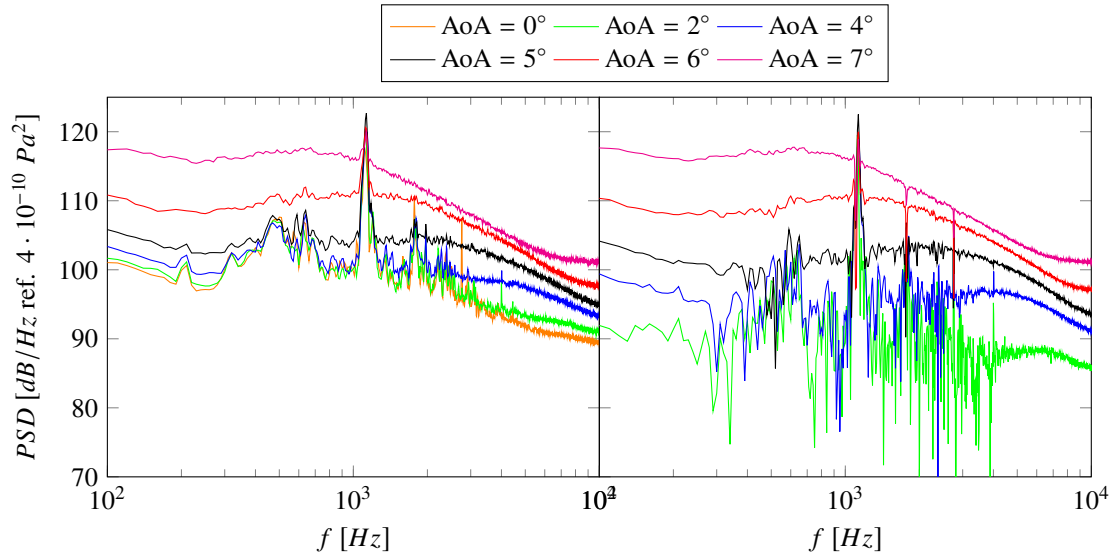


Fig. 1 Comparison of experimental wall surface pressure spectra at $\frac{x}{c} = 0.98$ for the CROR airfoil at $Ma = 0.55$ and $Re = 4$ Mio. before (left) and after (right) post-processing of the experimental data.

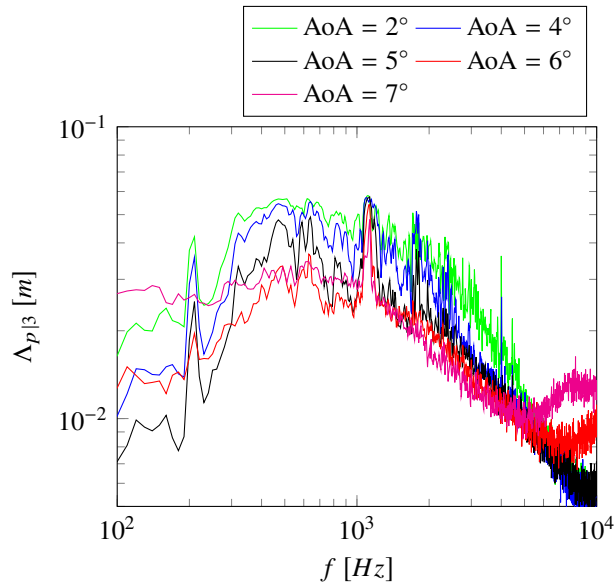


Fig. 2 Spanwise correlation length at $\frac{x}{c} = 0.98$ for the CROR airfoil at $Re = 4$ Mio. and $Ma = 0.55$.

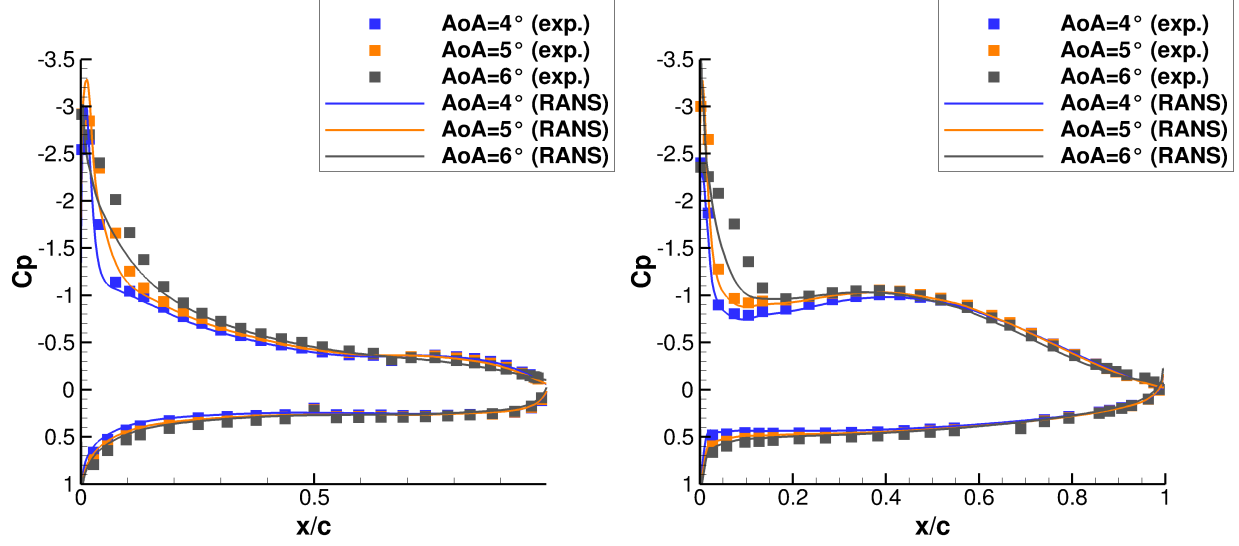


Fig. 3 Comparison of numerical (solid) and experimental (markers) pressure coefficients for the CROR airfoil at $Re = 4$ Mio. and $Ma = 0.55$ (left) and for the Valeo CD airfoil at $Re = 2.29$ Mio. and $Ma = 0.50$ (right).

γ between two unsteady pressure signals separated by a spanwise distance of $\Delta\xi_3$ is defined as

$$\gamma^2(\omega, \Delta\xi_3) = \frac{\langle p_w(x_1 = 0.98c, x_2 = 0, x_3, \omega) p_w^*(x_1 = 0.98c, x_2 = 0, x_3 + \Delta\xi_3, \omega) \rangle}{p_w(x_1 = 0.98c, x_2 = 0, x_3, \omega) p_w(x_1 = 0.98c, x_2 = 0, x_3, \omega)}. \quad (2)$$

The coherences of these spanwise sensors can then be used to determine the spanwise correlation length scale at 98% of the chord:

$$\Lambda_{p|3}(\omega) = \int_0^\infty \sqrt{\gamma^2(\omega, \Delta\xi_3)} d(\Delta\xi_3), \quad (3)$$

The resulting spanwise correlation length scales with respect to the frequency are shown for different angles of attack at a $Re = 4$ Mio. and $Ma = 0.55$ in Fig. 2. Note the resolution is not high as only a few microphone positions were used. Therefore, the results need to be regarded with caution. Furthermore, there seems to be some contamination of the signals at higher frequencies at high angles of attack. Following a peak in the spectra, all signals tend to feature a linear decrease in the logarithmic spanwise correlation length scale.

IV. CFD simulations

RANS simulations were performed to gain further insights into the flow on the airfoil surfaces and to extract inputs for the subsequently applied models for predicting the wall surface pressure autospectra near the trailing edge. Note that these inputs cannot be directly inferred from the experimental data set.

All RANS simulations were completed using the DLR in-house TRACE solver [37]. In this work, RANS solutions at different angles of attack were investigated for the following operating lines:

- CROR airfoil: $Re = 4.00$ Mio., $Ma = 0.38$
- CROR airfoil: $Re = 1.20$ Mio., $Ma = 0.55$
- CROR airfoil: $Re = 4.00$ Mio., $Ma = 0.55$
- Valeo CD airfoil: $Re = 2.29$ Mio., $Ma = 0.50$

For each simulation, the Menter Shear-Stress-Transport (SST) $k - \omega$ [38] turbulence model was applied. For selected operating points, other turbulence models including more complex differential Reynolds stress turbulence models were also applied to enable sensitivity studies. Variations in the Reynolds number were simulated analogous to the experiments - by adjusting the ambient pressure.

The RANS results were verified by comparing the numerical and experimental pressure coefficients as can be seen in Fig. 3. The overall agreement is satisfactory, although some discrepancies arise on the upper surface near the leading edge for both airfoils. This coincides with a growing flow detachment as the angle of attack increases. Fig. 4 depicts

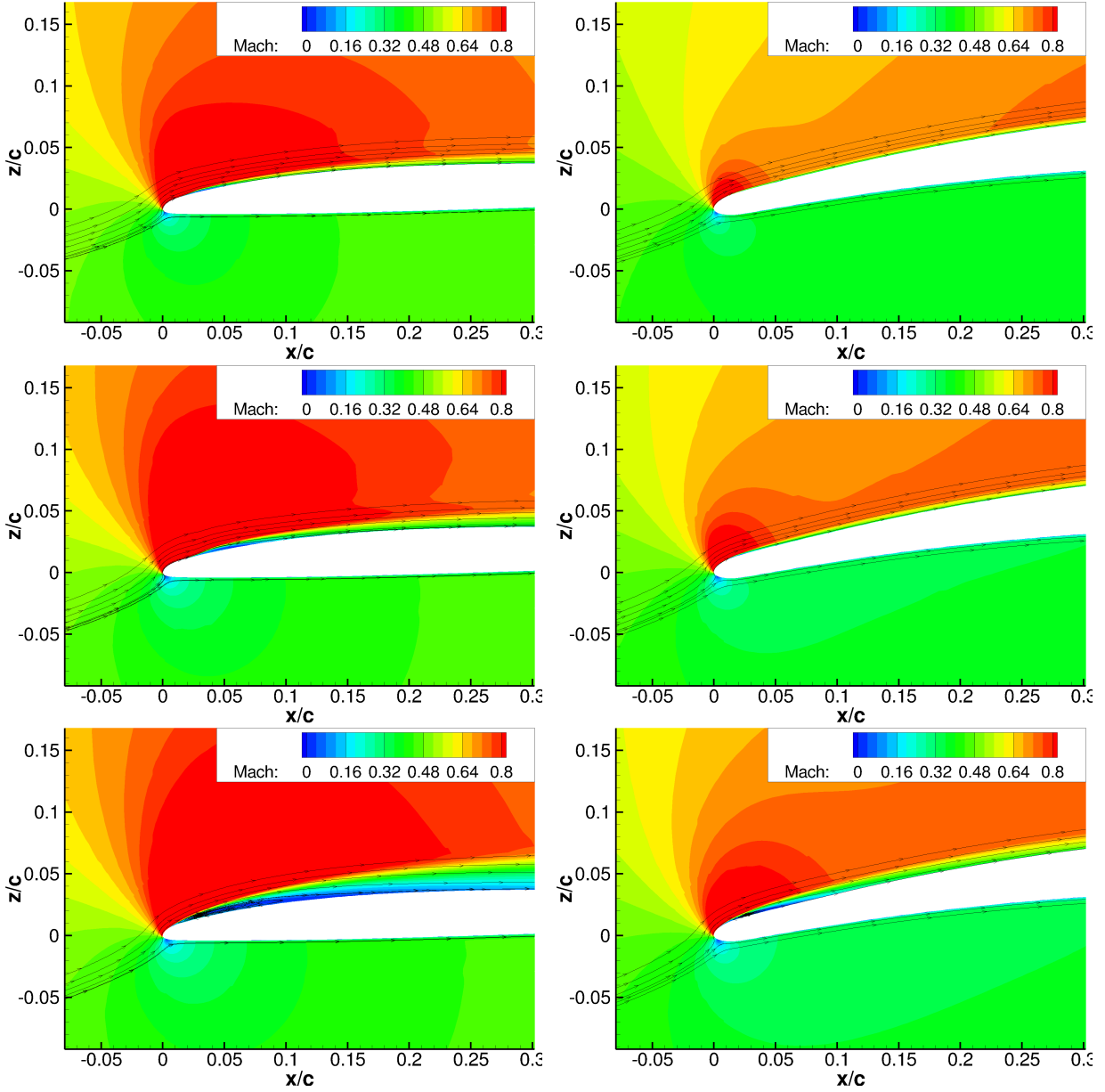


Fig. 4 Flow near the leading edge at $AoA = 4^\circ$ (top), $AoA = 5^\circ$ (center), and $AoA = 6^\circ$ (bottom) for the CROR airfoil at $Re = 4$ Mio. and $Ma = 0.55$ (left) and for the Valeo CD airfoil at $Re = 2.29$ Mio. and $Ma = 0.50$ (right).

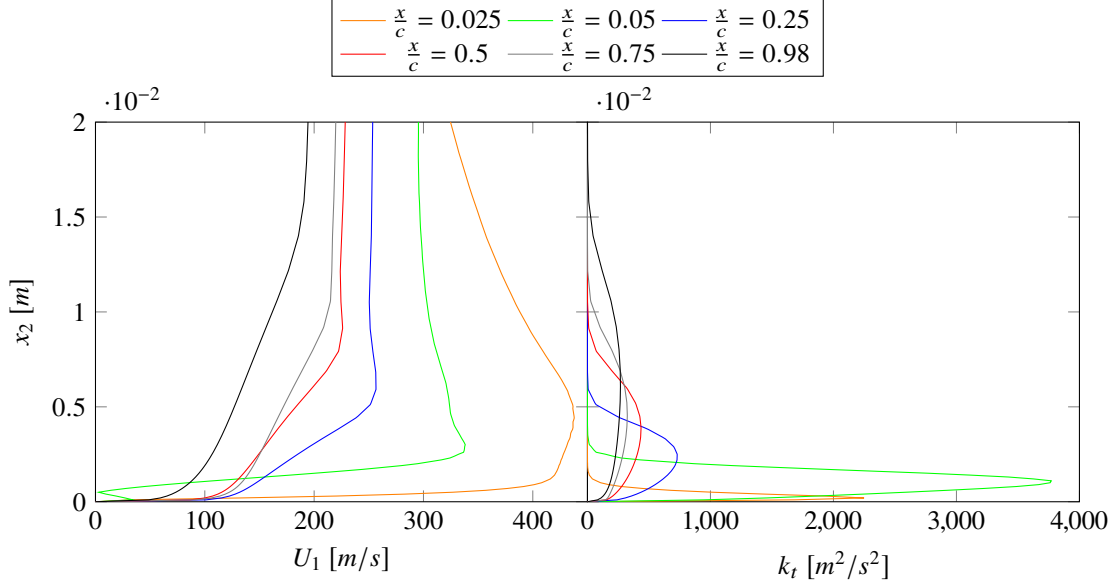


Fig. 5 Boundary layer profiles extracted from RANS at several axial positions for the CROR airfoil at AoA = 5°, Re = 4 Mio., and Ma = 0.55.

the flow at the leading edge of the airfoils at AoA = 4°, AoA = 5°, and AoA = 6° and shows the development of a pronounced flow detachment bubble with an increasing angle of attack. The recirculation zone is more pronounced for the CROR airfoil and results in a thicker boundary layer downstream of the recirculation zone. It should also be noted that such unsteady flow phenomena are difficult to capture using a steady RANS technique and that the chosen turbulence model also has a significant influence on the flow detachment.

The extraction of boundary layer parameters, which are needed as inputs for the wall pressure spectrum models, is not trivial for airfoils - especially at high angles of attack. As Weyburne [39] pointed out recently, the classical boundary layer theory is not applicable for airfoil flows. He distinguishes "bounded" boundary layer flows (equivalent to classical boundary layer theory), where the flow velocity gradually increases from zero at the wall surface to the free stream velocity at some distance from the wall, and "unbounded" boundary layer flows, which feature a peak velocity greater than the freestream velocity. "Bounded" boundary layers technically only occur in the presence of interacting pressure fields, induced by bounding walls, e.g in wind tunnels, pipes etc. For airfoils, the velocity peak due to the "unbounded" nature of the flow, i.e. the velocity peak in the boundary layer, tends to be quite pronounced a higher angles of attack towards the leading edge, as can be seen in Fig. 5 at chordwise positions of $\frac{x}{c} = 0.05$ and $\frac{x}{c} = 0.25$ at AoA = 5°. In other areas of the airfoil, the boundary layer profile resembles the classical boundary layer theory, e.g. at positions $\frac{x}{c} = 0.75$ and $\frac{x}{c} = 0.98$. Furthermore, the mean velocity profiles can include regions of flow detachment, e.g. at $\frac{x}{c} = 0.05$, and an additional velocity peak caused by strong flow accelerations, which can merge with the velocity peak of an "unbounded" boundary layer, e.g. at $\frac{x}{c} = 0.025$. Traditionally, the mean velocity or a derived quantity is used to extract the boundary layer thickness. However, the significant differences in the boundary layer profiles presents a challenge in formulating a robust algorithm for extracting boundary layer parameters. An alternative algorithm based on turbulent kinetic energy was therefore devised for this study. The boundary layer thickness was defined in terms of the percentage of the total turbulent kinetic energy contained in the boundary layer, specifically $\frac{\int_0^\delta k_t dx_2}{\int_0^\infty k_t dx_2} = 0.99$. This technique worked reliably for all RANS simulations, all tested turbulence models, and provided similar results as a more conventional algorithm based on the velocity profile. Compared to the algorithm based on total velocity, the algorithm based on the turbulent kinetic energy is more robust and requires fewer "engineering" parameters. The resulting boundary layer thicknesses for both CROR and Valeo CD airfoils are shown in Fig. 6.

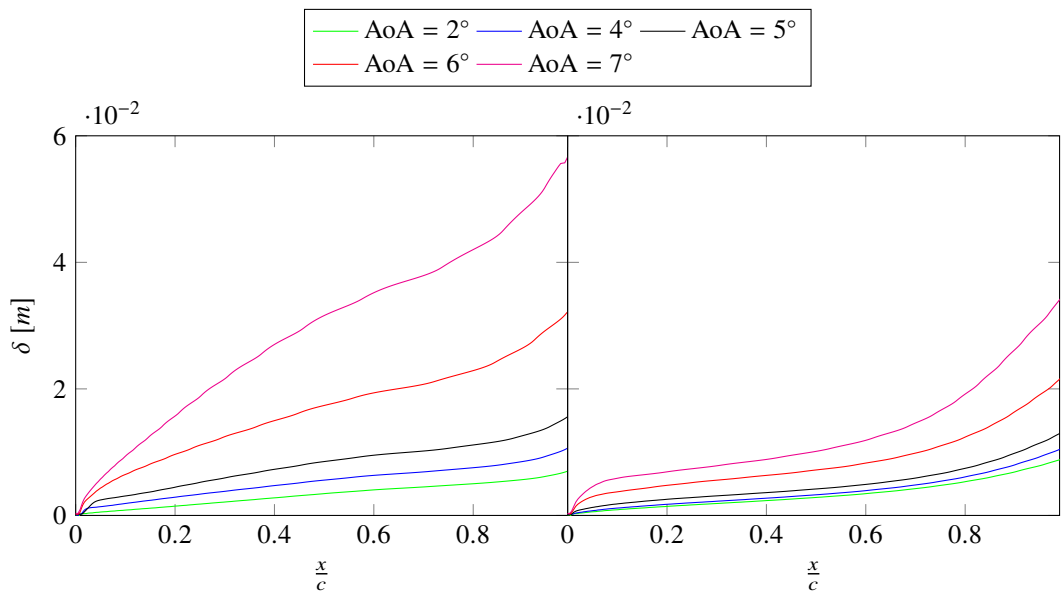


Fig. 6 Boundary layer thickness for the CROR airfoil at $Re = 4$ Mio. and $Ma = 0.55$ (left) and for the Valeo CD airfoil at $Re = 2.29$ Mio. and $Ma = 0.50$ (right).

Table 1 Spectral scaling factors SF , Strouhal numbers $\tilde{\omega}$, normalized spectra $MS(\tilde{\omega})$, and additional parameters used by investigated empirical models.

	SF	$\tilde{\omega}$	$MS(\tilde{\omega})$	additional parameters
WRA	$\frac{(\frac{1}{2}\rho_e U_e^2)^2 \delta^*}{U_e}$	$\frac{\omega \delta^*}{U_e}$	$\frac{2 \cdot 10^{-5}}{1 + \tilde{\omega} + 0.217\tilde{\omega}^2 + 0.00562\tilde{\omega}^4}$	
modified WRA			$\frac{C_D^2}{1 + \tilde{\omega} + 0.217\tilde{\omega}^2 + 0.00562\tilde{\omega}^4}$	
Goody	$\frac{\tau_w^2 \delta}{U_e}$	$\frac{\omega \delta}{U_e}$	$\frac{c_1 \tilde{\omega}^2}{[\tilde{\omega}^{0.75} + c_2]^{c_3} + [1.1R_T^{-0.57} \tilde{\omega}]^{c_4}}$	$c_1 = 3.0, c_2 = 0.5, c_3 = 3.7, c_4 = 7.0$
Rozenberg	$\frac{\tau_{max}^2 \delta^*}{U_e}$	$\frac{\omega \delta^*}{U_e}$	$\frac{c_1 \tilde{\omega}^2}{[4.76\tilde{\omega}^{0.75} + c_2]^{c_3} + [8.8R_T^{-0.57} \tilde{\omega}]^{c_4}}$	$c_1 = [2.82\Delta^2 (6.13\Delta^{-0.75} + c_2)^{c_3}] [4.2(\frac{\Pi}{\Delta}) + 1], c_2 = 4.76 \left(\frac{1.4}{\Delta}\right)^{0.75} [0.375c_3 - 1],$ $c_3 = 3.7 + 1.5\beta_C, c_4 = \min\left(3, \frac{19}{\sqrt{R_T}}\right) + 7$
Hu (v1)	$\frac{(\frac{1}{2}\rho_e U_e^2)^2 \theta}{u_\tau}$	$\frac{\omega \theta}{U_e}$	$\frac{c_1 \tilde{\omega}}{[\tilde{\omega}^{1.5(1.169 \ln H + 0.642)^{1.6} + c_2]^{c_3} + [7.645Re_\tau^{-0.411} \tilde{\omega}]^{c_4}}$	$c_1 = (81.004c_2 + 2.154) \cdot 10^{-7}, c_2 = 10^{-5.8e-5Re_\theta H - 0.35},$ $c_3 = 1.13/(1.169 \ln H + 0.642)^{0.6}, c_4 = 6$
Hu (v2)				$c_1 = (81.004c_2 + 2.154) \cdot 10^{-7}, c_2 = 0.07, c_3 = 1.13/(1.169 \ln H + 0.642)^{0.6}, c_4 = 6$
Lee	$\frac{\tau_w^2 \delta^*}{U_e}$	$\frac{\omega \delta^*}{U_e}$	$\frac{c_1 \tilde{\omega}^2}{[4.76\tilde{\omega}^{0.75} + c_2]^{c_3} + [8.8R_T^{-0.57} \tilde{\omega}]^{c_4}}$	$c_1 = \max((81.004c_2 + 2.154) \cdot 10^{-7}), (0.25\beta_C - 0.52) ((81.004c_2 + 2.154) \cdot 10^{-7}),$ $c_2 = \max(1, 1.5 (10^{-5.8e-5Re_\theta H - 0.35})), c_3 = 3.7 + 1.5\beta_C,$ $c_4 = \max(3, (0.139 + 3.1043\beta_C))$

V. Empirical models

Empirical models are commonly used for the modeling of wall surface pressure spectra, which can then be used as an input for the prediction of trailing edge noise. Empirical models are typically derived using experimental data sets. While these models can differ greatly, they follow the same generic principal:

$$\Phi_{pp}(\omega) = SF \cdot MS(\tilde{\omega}). \quad (4)$$

The wall surface pressure spectrum Φ_{pp} is scaled using a spectral scaling factor SF to collapse the spectrum to a normalized spectrum MS , which is defined as a function of a Strouhal number $\tilde{\omega}$. The Strouhal number is typically defined using boundary layer parameters.

Due to the sheer amount of available empirical models, only a selected number of models were examined in this paper:

- The **Willmarth-Roos-Amiet (WRA) model** was initially proposed by Willmarth and Roos [35] and subsequently adapted by Amiet [36]. The model is quite simple and relies strictly on outer boundary layer parameters, which means that the model is expected to fit better at lower frequencies. The model is restricted to Zero Gradient Pressure (ZPG) flows.
- A **modified WRA model** was proposed by Moreau [40]. He introduced the drag coefficient as an additional parameter. This is a unique feature as it is the only investigated model that relies on a global parameter, which describes the entire airfoil rather than only extracting local parameters at a specific position near the trailing edge.
- **Goody's model** [32] uses a combination of inner and outer boundary layer parameters but is also calibrated against a ZPG database.
- The **model of Rozenberg et al.** [33] was formulated on the basis of Goody's model and collapses to that initial formulation for ZPG cases. This model was, however, extended to consider Adverse Pressure Gradient (APG) effects, which can significantly increase the levels of the wall surface pressure autospectra for airfoils featuring high angles of attack.
- **Hu's model** [4] also uses Goody's model as a starting point. Contrarily to Rozenberg et al. [33], he chose a formulation which does not rely on the local pressure gradient $\frac{dp}{dx}$ but rather on the shape factor $H = \frac{\delta^*}{\theta}$. The shape factor is a parameter which is representative for the development history of the boundary layer history. Another advantage of this model is that its variables are independent in that each variable influences exactly one feature of the spectral shape. However, Hu proposed two different formulations in his paper, which result in the same spectrum for his database but this is not necessarily true for all cases.
- **Lee's model** [5] is an extension of the model of Rozenberg et al. [33]. This new formulation was proposed to be suitable for many different flow conditions.

The used formulations of these empirical models are listed in terms of the generic equation Eq. 4 in Table 1.

Fig. 7 depicts the results of the empirical models for the CROR and Valeo CD airfoils at $AoA = 4^\circ$, $AoA = 5^\circ$, and $AoA = 6^\circ$. None of the investigated empirical models seems to be capable of reproducing the experimental spectra or even capturing experimental trends robustly. While this is to be expected for ZPG models (WRA, Goody), the performance of the models (Rozenberg, Hu, Lee), which are specifically formulated for APG flows, is also disappointing. One key difference between the investigated data sets in this paper is that Reynolds (0.9 - 4.0 Mio.) and Mach numbers (0.38 - 0.55) are representative for a full-scale aeroengine. Databases, which were used to calibrate existing empirical models, feature significantly lower Reynolds (1-2 order of magnitude lower) and Mach numbers (approx. 0.05 - 0.2). As Reynolds and Mach numbers are driving factors for the behavior of the boundary layer, it is likely that these also have a significant influence of wall surface pressure autospectra. It is possible that these cases with such high Reynolds and Mach numbers are simply outside the range of validity of the applied empirical models. For the completeness, it should also be re-mentioned at this point that the experimental data does feature some signal contamination, which can also be a source of uncertainty.

The WRA and Goody models were formulated exclusively for ZPG flow cases. Both models are therefore expected to result in significantly lower spectral levels. Nonetheless, the offset between the models are significant for all cases. In contrast, the modified WRA model overshoots the experimental values significantly. While the idea of introducing a global value to scale the normalized spectrum is certainly an interesting one, it does not seem to have reached a sufficient maturity. With the added consideration of the APG, the models tend to become increasingly more complex and involve an abundance of boundary layer parameters as can be seen in Table 1. The complexity and the boundary layer parameters, which need to be extracted from CFD simulations, can adversely influence the robustness of the models. This is especially critical if one intends to apply the models in the context of design optimization schemes. If the objective were to expand one of the investigated APG models to high Reynolds and Mach number cases, the authors

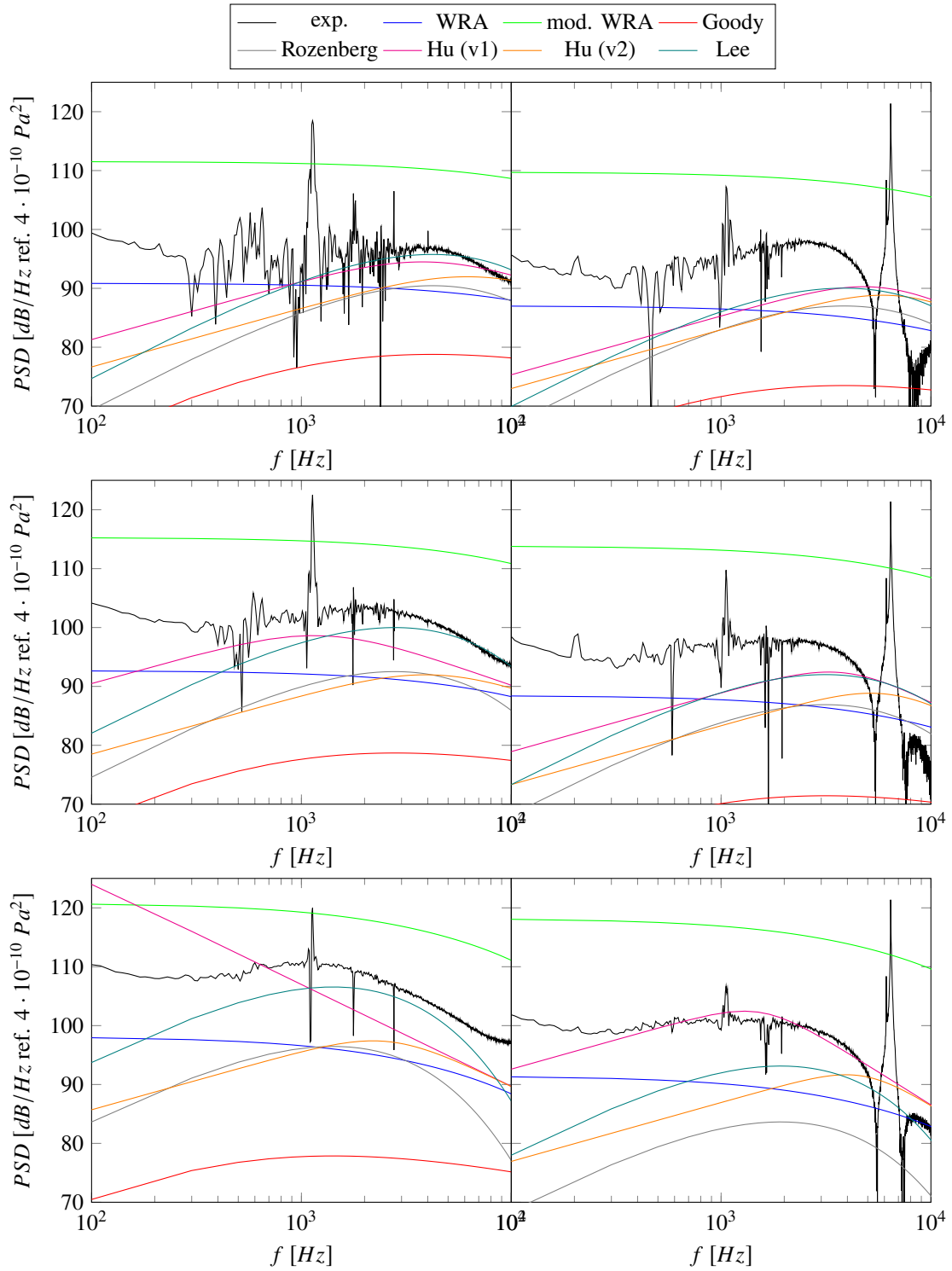


Fig. 7 Comparison of experimental and empirical wall surface pressure spectra at $\text{AoA} = 4^\circ$ (top), $\text{AoA} = 5^\circ$ (center), and $\text{AoA} = 6^\circ$ (bottom) at $\frac{x}{c} = 0.98$ for the CROR airfoil at $\text{Re} = 4 \text{ Mio.}$ and $\text{Ma} = 0.55$ (left) and for the Valeo CD airfoil at $\text{Re} = 2.29 \text{ Mio.}$ and $\text{Ma} = 0.50$ (right).

would recommend to use Hu’s model (v1) as a baseline. While it clearly performs differently for the studied cases in this paper than for the cases investigated by Hu [4] (e.g. for the CROR and Valeo CD airfoils, the two formulations of the model do not collapse to nearly the same curve), the model has some advantages: 1.) The model is rather robust, whereas the Lee and Rozenberg models yield no solution in regions of detached flows. This presents a challenge for the CROR airfoil, which features a bubble of separated flow near the trailing edge at high angles of attack. While the validity of the models is certainly questionable for cases with detached flow, discontinuities due to a ‘nan’ value can be highly destructive in automatized procedures. 2.) The parameters of the normalized spectrum are not interdependent and each variable specifically influences one feature of the spectrum. This is an interesting feature, especially if the aim is to expand the model. However, given that there does seem to be a dependency on the data set used to calibrate empirical model, it may be difficult to define empirical models, which are valid for a very wide variety of cases.

VI. Stalnov TNO model

The discussions and analyses in the previous section have shown that empirical models for the prediction of wall surface pressure autospectra are not well suited for the studied cases, which feature high Reynolds and Mach numbers. Therefore, an alternative approach, namely the TNO model by Stalnov et al. [28], is the focus of this section. TNO models follow a different approach to empirical models in that they aim to approximate the solution of the Poisson equation (Eq. 1) using simplified, analytical formulations. TNO models typically neglect the turbulence-turbulence-interaction term and focus on solving the mean shear term. However, TNO models still rely on simplifying assumptions. The impact of these assumptions are investigated in the first part of this section. Furthermore, RANS-based TNO models (and empirical models) also depend on CFD simulation settings, specifically the choice of the turbulence model can have a significant impact on the predicted spectrum. The sensitivity of the predicted wall surface pressure autospectrum will therefore be discussed in this section. Lastly, the experimental versus predicted trends are studied and discussed.

A. Analysis of sensitivities due to empirical assumptions

The TNO model by Stalnov et al. [28] can be formulated as follows:

$$\Phi_{pp}(\omega) = \frac{4\pi\rho_e^2}{\Lambda_{p|3}(\omega)} \int_0^\delta \Lambda_{2,22}(x_2) U_c(x_2) \left[\frac{\partial U_1(x_2)}{\partial x_2} \right]^2 \frac{\overline{u_2^2(x_2)}}{U_c^2(x_2)} \phi_{22} \left(k_1 = \frac{\omega}{U_c(x_2)}, k_3 = 0 \right) e^{-2x_2 \frac{\omega}{U_c(x_2)}} dx_2, \quad (5)$$

where the transverse fluctuating velocity spectrum $\phi_{22} \left(k_1 = \frac{\omega}{U_c(x_2)}, k_3 = 0 \right)$ is defined as

$$\phi_{22} \left(k_1 = \frac{\omega}{U_c(x_2)}, k_3 = 0 \right) = \frac{4}{9\pi} \frac{\beta_1 \beta_3}{k_e^2} \frac{(\beta_1 k_1 / k_e)^2}{[1 + (\beta_1 k_1 / k_e)^2]^{7/3}}. \quad (6)$$

To perform an analysis with respect to empirical assumptions needed to solve Eq. 5, an initial formulation was implemented using the following assumptions:

- Convective mean velocity U_c : The convective mean velocity was assumed to be a constant, i.e $U_c = 0.65U_e$.
- Spanwise correlation length scale $\Lambda_{p|3}(\omega)$: The model of Corcos [30] was applied: $\Lambda_{p|3}(\omega) = \frac{U_c}{\alpha\omega}$, where the constant α is equal to 0.714. Note that the model of Corcos cannot produce realistic spanwise correlation lengths at lower frequencies.
- Turbulence parameters:
 - Turbulent length scale $\Lambda_{2,22}$ perpendicular to the blade surface: The transverse length scale $\Lambda_{2,22}$ was determined as a function of the integral length scale Λ : $\Lambda_{2,22}(x_2) = 0.5\Lambda(x_2)$. Note that this formula is technically only true for the case of homogeneous, isotropic turbulence, not for anisotropic turbulence in a boundary layer. In contrast to Stalnov et al. [28], who determined the integral length scale based on the mixing length scale and further corrected it by the Klebanoff damping function [41] near the boundary layer edge, the integral length scale was directly extracted from the RANS equation in this work by using a formulation proposed by Pope [42]: $\Lambda(x_2) = \frac{C_{Re}}{C_\mu} \frac{\sqrt{k_t(x_2)}}{\omega_t(x_2)}$. Note that the constant $C_\mu = 0.09$ depends on the formulation of the turbulence model and the constant C_{Re} depends on the Reynolds number. The latter constant was set to a value of 0.4 as Donzis et al. [43] showed that the value asymptotically approaches 0.4 for high Reynolds numbers.

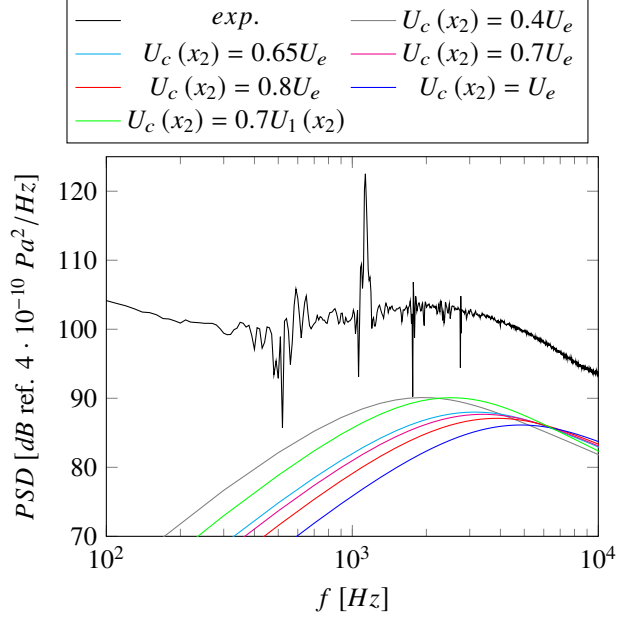


Fig. 8 Impact of the definition of the convective mean velocity in the TNO Stalnov model on the predicted wall surface pressure spectrum for the CROR airfoil at AoA = 5°, Re = 4 Mio., and Ma = 0.55.

- Anisotropic stretching factors $\beta_i = \frac{\overline{u_i^2}}{\overline{u_1^2}}$ and mean squared fluctuating transverse velocity $\overline{u_2^2}(x_2)$: Stalnov et al. [28] applied values of $\beta_1 = 1.0$, $\beta_2 = 0.5$ and $\beta_3 = 0.75$. Consequently, the mean squared fluctuating transverse velocity can be formulated in terms of the turbulent kinetic energy k_t , extracted from the RANS simulation, and the anisotropic stretching factors: $\overline{u_2^2}(x_2) = 2k_t \frac{\beta_2}{\beta_1 + \beta_2 + \beta_3}$.

All sensitivity studies were performed for the design point of the CROR airfoil at AoA = 5°, Re = 4 Mio., and Ma = 0.55.

1. Convective mean velocity

The convective velocity U_c refers to the convective speed of the eddies in the boundary layers. The convective velocity is oftentimes defined in terms of the boundary layer edge velocity $U_c(x_2) = cU_e$, where the constant can vary between values of 0.4 to 1.0. A constant c of 0.8 as suggested by Amiet is commonly used. However, recent studies have shown that the convective velocity may actually be lower. In fact, Del Alamo and Jimenez [44] analyzed the boundary layer of DNS simulation and found that smaller eddies in wall proximity convected at 40% of the mean velocity of the channel. Larger eddies near the edge of the boundary layer convected at 70% of the mean velocity of the channel. In light of these findings, it may be a valid idea to formulate the convective velocity in terms of the mean flow velocity in the boundary layer $U_c(x_2) = cU_1(x_2)$. The convective velocity is therefore smaller in the lower layers of the boundary layer and converges to the formulations in terms of the boundary layer edge velocity for the outer layer of the boundary layer.

Fig. 8 depicts the impact of the definition of the convective mean velocity on the predicted wall surface pressure spectrum. If the overall convective velocity decreases, the spectral levels increase and the frequency peak is shifted towards a lower frequency. For the subsequent analyses, the convective mean velocity was defined as $U_c(x_2) = 0.7U_1(x_2)$. Not only does this definition account for the fact that differently sized eddies convect with a different speed but the spectral shape of the predicted wall surface pressure spectrum also corresponds well with the experimental data set. Nonetheless, a significant offset between experimental and predicted spectral levels remains.

2. Spanwise correlation length scale

There are a number of different formulations for the spanwise correlation length $\Lambda_{p|3}(\omega)$. Besides the previously mentioned formulation of Corcos [30], the following other commonly used formulations are investigated in this work:

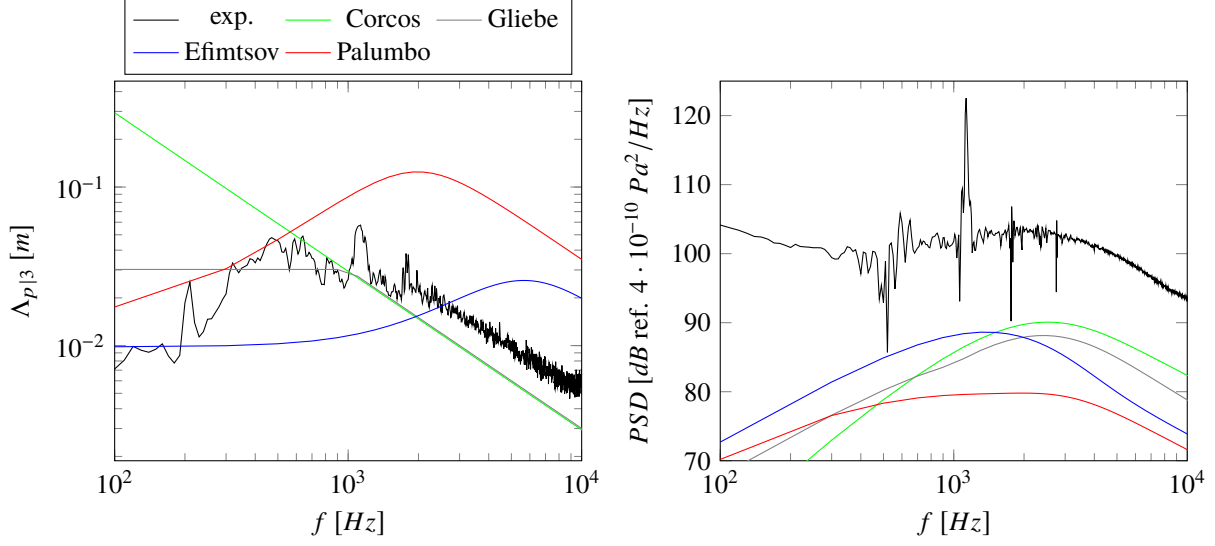


Fig. 9 Impact of the definition of the spanwise correlation length scale in the TNO Stalnov model on the predicted wall surface pressure spectrum for the CROR airfoil at $\text{AoA} = 5^\circ$, $\text{Re} = 4 \text{ Mio.}$, and $\text{Ma} = 0.55$.

- Gliebe [45] proposed a definition of the spanwise correlation length scale as a function of the wake width δ_w , which can be assumed to be approximately equal to twice the boundary layer thickness δ near the trailing edge. The spanwise correlation length scale is defined as follows:

$$\begin{aligned}
 - \Lambda_{p|3}(\omega) &= \delta_w \forall \frac{\omega \delta_w}{U_e} < 1 \\
 - \Lambda_{p|3}(\omega) &= \delta_w \left(\frac{1}{\frac{\omega \delta_w}{U_e}} \right) \forall \frac{\omega \delta_w}{U_e} > 1
 \end{aligned}$$

- Efimtsov [46] defined the spanwise correlation length scale as follows: $\Lambda_{p|3}(\omega) = \delta \left[\left(\frac{a_1 \left(\frac{\omega \delta}{u_\tau} \right)}{U_c / u_\tau} \right)^2 + \frac{a_2^2}{\left(\frac{\omega \delta}{u_\tau} \right)^2 + (a_2/a_3)^2} \right]^{-1/2}$

with $a_1 = 0.1$, $a_2 = 72.8$, and $a_3 = 1.54$. Palumbo [47] later proposed re-calibrated, Mach number-dependent coefficients. He recommended the constants $a_1 = 0.06$, $a_2 = 5.0$, and $a_3 = 1.0$ for the case of $\text{Ma} = 0.56$, which is most similar to the investigated CROR airfoil at $\text{Ma} = 0.55$. Note that due to the dependency of the model on u_τ , no solution can be expected for cases featuring detached flow. This presents a challenge as it adversely impacts the robustness of the overall method.

The comparison of predicted and experimental wall surface pressure spectra and spanwise correlation length scales are shown in Fig. 9. The Efimtsov and Palumbo models deviate significantly from the experimentally determined spanwise correlation length scales. The Corcos and Gliebe models are very similar at higher frequencies. At lower frequencies, the Gliebe model remains constant. In the subsequent analyses, the Gliebe model was applied as it seems to be the most reasonable fit for the investigated case.

3. Turbulence parameters

The wall surface pressure spectrum depends on the boundary layer turbulence. However, quantifying the anisotropic nature of the boundary layer turbulence using relatively simple formulations is a challenge. Anisotropic behavior can be introduced using the following variables: the transverse length scale $\Lambda_{2,22}$ or the transverse correlation length scale $L_{2,22}$, the mean squared fluctuating transverse velocity $\overline{u_2^2}(x_2)$, and by introducing anisotropy factors β_i to modify the normalized, von Kármán transverse velocity spectrum in Eq. 6. The von Kármán velocity spectrum in its unmodified form is only valid for the description of homogeneous, isotropic turbulence. The following combinations of turbulence parameters are studied:

- reference (based on Stalnov et al. [28], described towards the beginning of this section): $\Lambda_{2,22}(x_2) = 0.5\Lambda(x_2)$, $\beta_1 = 1.0$, $\beta_2 = 0.5$, $\beta_3 = 0.75$, $\overline{u_2^2}(x_2) = 2k_t \frac{\beta_2}{\beta_1 + \beta_2 + \beta_3} \approx 0.44k_t$

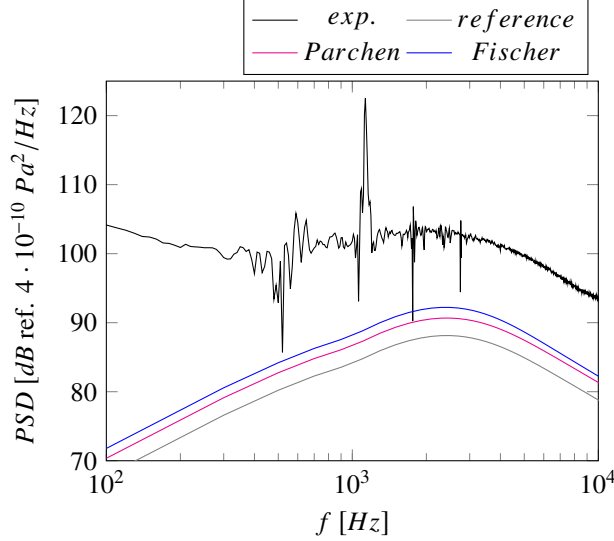


Fig. 10 Impact of the definition of the turbulence characteristics in the TNO Stalnov model on the predicted wall surface pressure spectrum for the CROR airfoil at AoA = 5°, Re = 4 Mio., and Ma = 0.55.

- Parchen [24]: $\Lambda_{2,22}(x_2) = \frac{\sqrt{\pi}\Gamma(\frac{5}{6})}{\Gamma(\frac{1}{3})}\Lambda(x_2) \approx 0.747\Lambda(x_2)$, $\beta_1 = 1.0$, $\beta_2 = 0.74$, $\beta_3 = 0.9$, $\overline{u_2^2}(x_2) = 0.45$
- Fischer et al. [29]: $L_{2,22}(x_2, \omega) = \frac{\sqrt{\pi}\Gamma(\frac{1}{3})}{3\Gamma(\frac{5}{6})}\Lambda(x_2)\beta_2\frac{3+11\eta_c^2}{3+8\eta_c^2}\frac{1}{\sqrt{1+\eta_c^2}}$ with $\eta_c = \beta_1\Lambda(x_2)\frac{\omega}{U_c}$, $\beta_1 = 1.0$, $\beta_2 = 0.74$, $\beta_3 = 0.9$, $\overline{u_2^2}(x_2) = 0.44k_t$

Fig. 10 depicts the impact of the used turbulence characteristics on the wall surface pressure autospectra. For the investigated case, the spectral shape does not change significantly but the absolute spectral levels vary. As the parameters applied by Fischer et al. [29] decrease the offset between experimental and predicted spectral levels, these parameters were applied in subsequent analyses. One inconsistency regarding the parameters proposed by Fischer et al. [29] should, however, be pointed out. If the anisotropic stretching factors are defined as $\beta_i = \frac{\overline{u_i^2}(x_2)}{u_1^2(x_2)}$, it should be possible to compute $\overline{u_2^2}(x_2)$ in terms of the anisotropic stretching factors and the turbulent kinetic energy. However, $2k_t\frac{\beta_2}{\beta_1+\beta_2+\beta_3} \approx 0.56k_t \neq 0.44k_t$.

B. Analysis of sensitivities due to chosen turbulence model

With all RANS-informed models, the results of the Stalnov TNO model also depend on the applied RANS simulation settings. Kissner et al. [48] have recently performed an in-depth investigation of the dependency of predicted fan broadband noise on the RANS simulation and pointed out that the choice in turbulence model is a key influencing factor. The following turbulence models were applied for the design point of the CROR airfoil to quantify the uncertainty of the model due to the use of different turbulence models: Wilcox $k - \omega$ [49], Menter SST $k - \omega$ [38], Hellsten EARSM $k - \omega$ [50], Wilcox stress- ω [51], SSG/LRR- ω [52], and JH stress- ω^h [53–55].

Fig. 11 shows the influence of the turbulence model on the modeled wall surface pressure autospectra. The investigated case features a flow separation bubble near the leading edge. Such unsteady flow phenomena are challenging to simulate using RANS techniques and are particularly sensitive with respect to the turbulence model. Since the flow separations and subsequent flow reattachment influence the behavior of the boundary layer, the influence of turbulence models is expected to be non-negligible, which is confirmed in Fig. 11. The choice in turbulence impacts the spectral levels, especially at low to mid frequencies, and shifts the frequency peak. At higher frequencies, the different solutions behave similarly. Note that it is difficult to determine the "right" choice for turbulence model based on the given information. The intent is to simply provide a quantitative depiction of uncertainties due to the RANS simulation. The Menter SST $k - \omega$ model was used for all other simulations in this work.

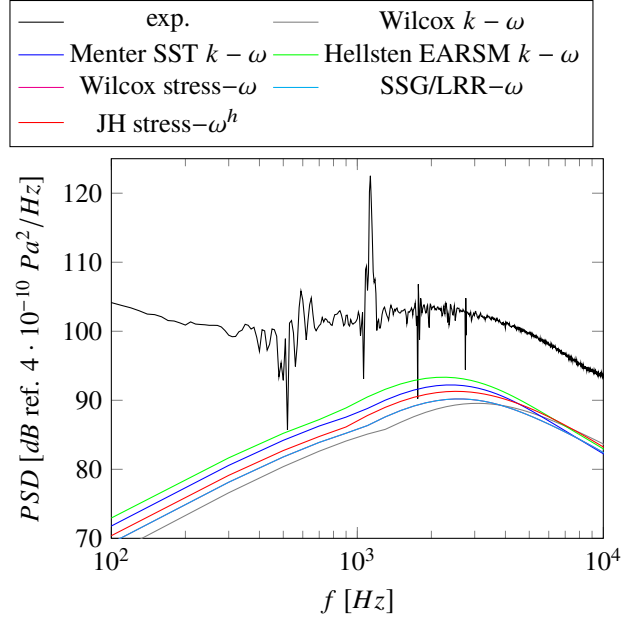


Fig. 11 Impact of the definition of the turbulence model on the predicted wall surface pressure spectrum for the CROR airfoil at $\text{AoA} = 5^\circ$, $\text{Re} = 4 \text{ Mio.}$, and $\text{Ma} = 0.55$.

C. Analysis of trends

A comparison of experimental and predicted wall surface pressure autospectra is shown in Fig. 12. In contrast to the empirical models, the trends in terms of the spectral shape look promising for both CROR and Valeo CD airfoils. The position of the frequency peaks are well captured - at least for $\text{AoA} = 4^\circ$ and $\text{AoA} = 5^\circ$. It stands to reason that the model becomes less accurate as the flow recirculation domain near the blade leading edge becomes increasingly relevant. At lower frequencies, the experimental results are likely contaminated and difference in spectral shape at these frequencies is therefore expected.

Despite performing a number of sensitivity studies and repeatedly checking the implementation of the model as well as the post-processing routines for the experimental data, there still exists a fairly consistent offset between experimental and predicted spectral levels. To improve and further check the Stalnov TNO model, the authors suggest to reexamine the empirical assumptions used by the model, especially the parameters describing the anisotropy in the turbulent boundary layer. Scale-resolving, high-fidelity simulations could potentially be helpful to further investigate the CROR and Valeo CD airfoils.

Figures 13, 14, and 15 compare the experimental and predicted trends in wall surface pressure autospectra with respect to variations in the Reynolds number, Mach number, and chordwise position. Some observations:

- As in previous analyses, the model seems to become less reliable at higher angles of attack, where flow separations become increasingly dominant. The frequency peaks are not captured well and the slope becomes very steep at high frequencies. Since flow separations are more difficult to compute using RANS techniques so there is some uncertainty arising from the RANS-informed inputs as well.
- A mismatch at lower frequencies is expected due to signal contamination in the measurement data.
- At high frequencies, the measurement data feature relatively similar slopes. This contrasts the behavior of the predicted spectra, which feature discernibly different slopes at high frequencies.
- Except for cases featuring more pronounced recirculation domains at high angles of attack, the experimental and predicted offsets feature a similar magnitude.
- Deviations with respect to chordwise position are small for both measured and predicted spectra in proximity to the blade trailing edge. This is reassuring and confirms a certain robustness of the Stalnov TNO method.

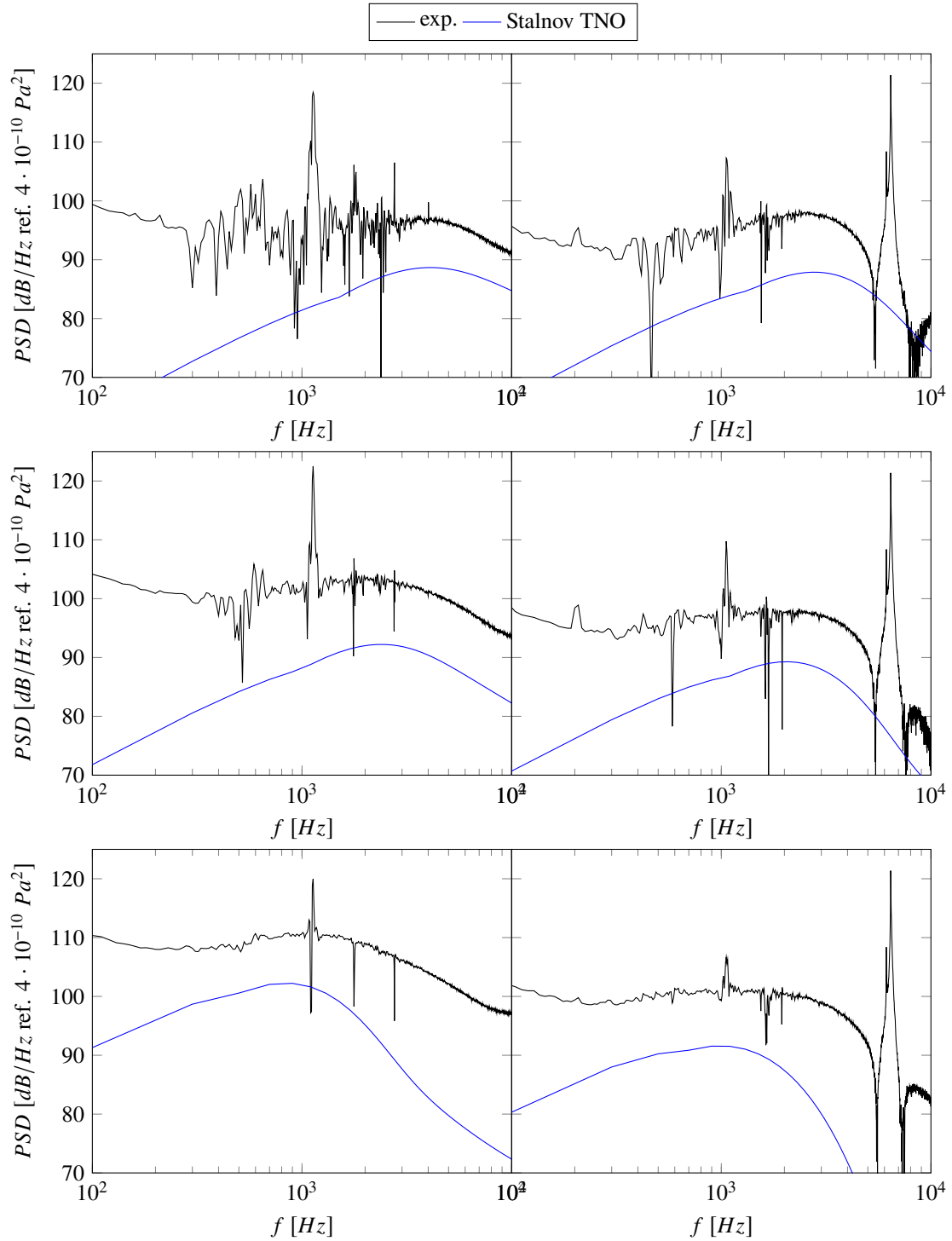


Fig. 12 Comparison of experimental and Stalnov TNO wall surface pressure spectra at $\text{AoA} = 4^\circ$ (top), $\text{AoA} = 5^\circ$ (center), and $\text{AoA} = 6^\circ$ (bottom) at $\frac{x}{c} = 0.98$ for the CROR airfoil at $\text{Re} = 4 \text{ Mio.}$ and $\text{Ma} = 0.55$ (left) and for the Valeo CD airfoil at $\text{Re} = 2.29 \text{ Mio.}$ and $\text{Ma} = 0.50$ (right).

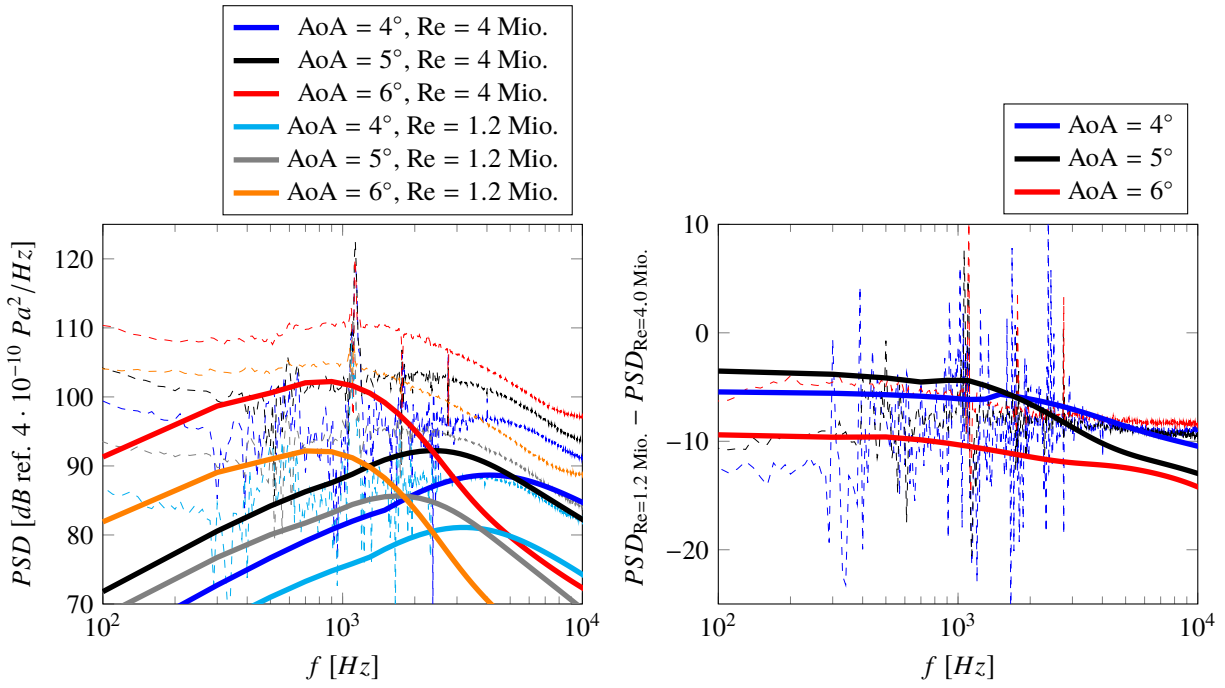


Fig. 13 Comparison of experimental and Stalnov TNO trends for the CROR airfoil with respect to variations in Reynolds number at $\frac{x}{c} = 0.98$ and $\text{Ma} = 0.55$.

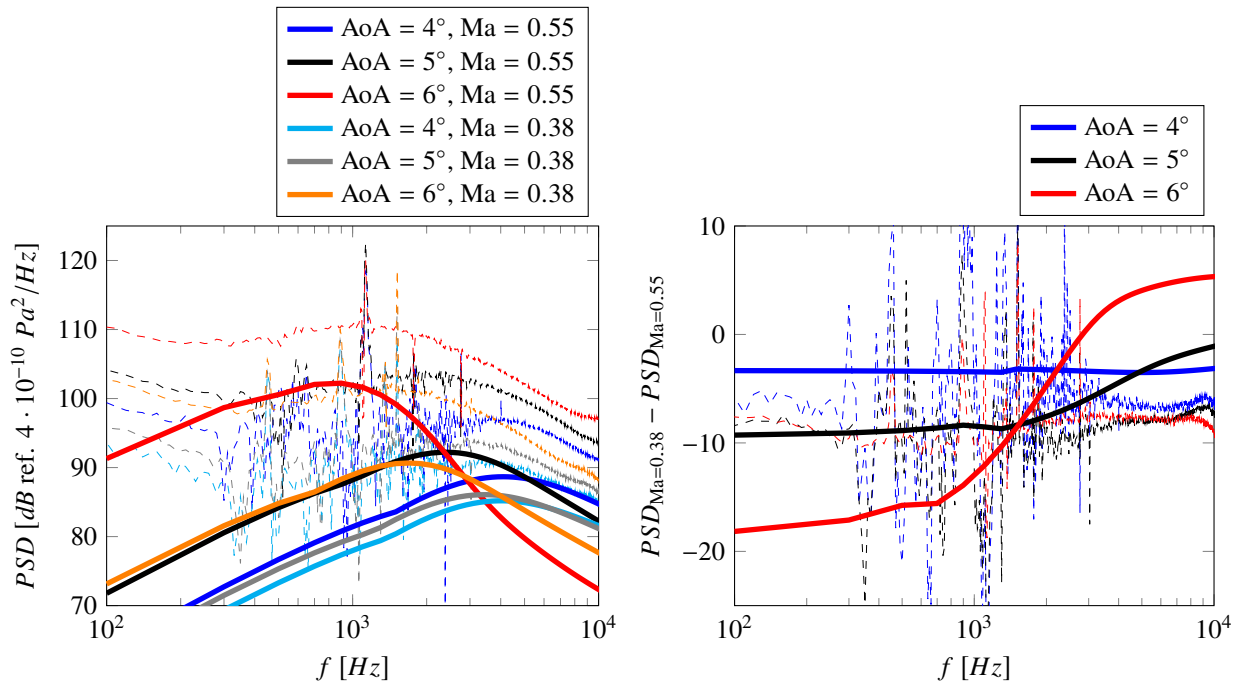


Fig. 14 Comparison of experimental and Stalnov TNO trends for the CROR airfoil with respect to variations in Mach number at $\frac{x}{c} = 0.98$ and $\text{Re} = 4 \text{ Mio.}$

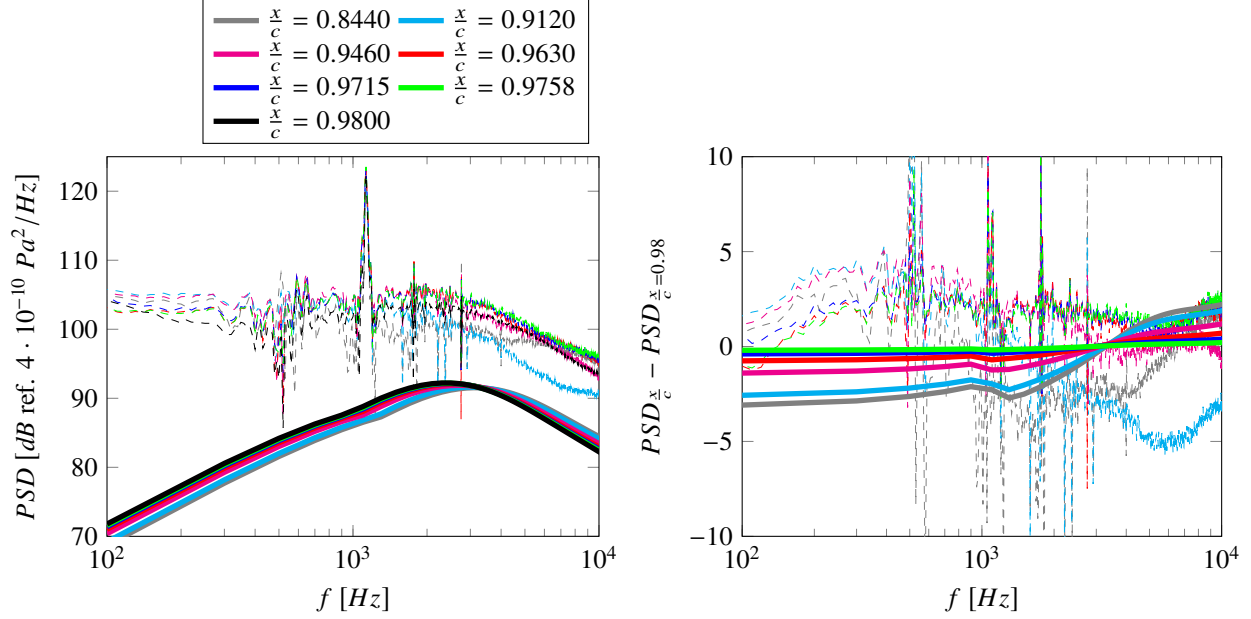


Fig. 15 Comparison of experimental and Stalnov TNO trends for the CROR airfoil with respect to variations in chordwise position at AoA = 5°, Ma = 0.55 and Re = 4 Mio.

VII. Conclusion

The key ingredient for the prediction of trailing edge broadband noise is the accurate modeling of the wall surface pressure trailing edge. However, there is no consensus within the scientific community on one modeling approach and therefore numerous models exist. This paper followed an engineering approach and investigated selected RANS-informed empirical models and the Stalnov TNO model to the CROR and Valeo CD airfoils. The aim was to analyze the models with respect to their accuracy and suitability for an integration into fast and robust noise modeling tools, which can be used within optimization schemes to enable silent UHBR and CROR designs. In contrast to the majority of studies concerning the modeling of wall surface pressure spectra for trailing edge noise prediction, this work examined test cases at realistic Reynolds and Mach numbers as opposed to the much lower Reynolds and Mach numbers typically used in academic test cases.

Steady and unsteady pressure data, measured in the DNW-TWG wind tunnel, were used to evaluate the validity of the RANS simulations and to analyze the modeled wall surface pressure autospectra. RANS simulations were performed on different operating lines and enabled the determination of boundary layer parameters, which are needed as input for empirical models and the Stalnov TNO model. Note that boundary parameters cannot be directly determined from the experimental data. The RANS data indicated that areas of flow recirculation appear near the leading edges of both airfoils at higher angles of attack. Such a flow detachment has a significant influence on the boundary layer downstream of the recirculation zone. In general, the boundary layer flow proved to be complex, featuring characteristics typical of "unbounded" boundary layers, strong flow accelerations on the upper blade surface, and the aforementioned recirculation zone. To increase the robustness of the algorithm for extracting boundary layer parameters, the authors proposed an approach based on the turbulent kinetic energy rather than the total velocity or related quantities.

The following empirical models were implemented and investigated: Willmarth-Roos-Amiet, modified Willmarth-Roos-Amiet, Goody, Rozenberg, Hu, and Lee. Even though these models work well for academic cases as shown by a large number of authors, all models failed to reproduce the experimental wall surface pressure autospectra and to capture experimental trends. One possible explanation is that the investigated cases of this work differ too strongly from the academic databases, which are typically used to calibrate/inform the empirical models. In fact, the investigated flight Reynolds (0.9 - 4.0 Mio.) and Mach numbers (0.38 - 0.55) of the analyzed cases were significantly higher than Reynolds (1-2 order of magnitude lower) and Mach numbers (approx. 0.05 - 0.2) of commonly used databases. If the aim were to adapt one of the investigated empirical models for realistic turboengine conditions, Hu's model seems like the most promising candidate as it proved to be robust and the parameters of the normalized spectrum have the advantage of influencing only one respective aspect of the spectral shape. Nonetheless, improving/expanding an existing model to

deliver consistent predictions for the investigated cases may not be the most reasonable approach as the resulting model may then be limited to specific use cases as formulating universal empirical models seems to be unlikely.

TNO models follow a different approach with the aim of solving the Poisson equation. The resulting formulations are more complex than for most empirical models but are still simple enough for the potential integration into fast acoustic prediction tools. Due to simplifying assumptions, these models, however, still contain some empirical values to describe the convective mean velocity, the spanwise correlation length scale, and turbulence parameters of the boundary layer. The impact of these sensitivities on the wall surface pressure spectra were studied in detail for the design point of the CROR airfoil using the Stalnov TNO model. The most reasonable parameters ($U_c(x_2) = 0.7U_1(x_2)$; $\Lambda_{p|3}(\omega) = \delta_w \sqrt{\frac{\omega \delta_w}{U_e}} < 1$ and $\Lambda_{p|3}(\omega) = \delta_w \frac{1}{\left(\frac{\omega \delta_w}{U_e}\right)} \sqrt{\frac{\omega \delta_w}{U_e}} > 1$; $L_{2,22}(x_2) = \frac{\sqrt{\pi} \Gamma\left(\frac{1}{3}\right)}{3\Gamma\left(\frac{5}{6}\right)} \Lambda(x_2) \beta_2 \frac{3+11\eta_c^2}{3+8\eta_c^2} \frac{1}{\sqrt{1+\eta_c^2}}$ with $\eta_c = \beta_1 \Lambda(x_2) \frac{\omega}{U_c}$, $\beta_1 = 1.0$, $\beta_2 = 0.74$, $\beta_3 = 0.9$, $u_2^2(x_2) = 0.44k_t$) were chosen for the investigated case. Note that these parameters are not necessarily transferable to other cases.

While the Stalnov TNO model performs significantly better in capturing the spectral shape and trends compared to the investigated empirical models, an offset between experimental and predicted wall surface pressure autospectra persists and cannot be explained by the performed sensitivity studies. Nonetheless, the authors suggest to reexamine the empirical assumptions in future works, especially the parameters concerning the description of the anisotropic behavior of the turbulent boundary layer. Comparisons with statistical methods for predicting the wall surface pressure autospectra and performing scale-resolving, high-fidelity simulations to gain insights into the behavior of the boundary layer may be helpful for further improving the performance of the Stalnov TNO model. In fact, Boukharfane et al. [11] applied an LES technique for the Valeo CD at the same experimental conditions as discussed in this work and achieved an acceptable agreement between numerical and experimental wall surface pressure spectra. This suggests that advanced numerical methods can reproduce experimental results for cases featuring high Reynolds and Mach numbers and can therefore potentially be used to improve analytical models.

Even though the Stalnov TNO model proved to be robust and fast during this study - even compared to very simple empirical models, it may be necessary to simplify the model before integrating it into complex optimization schemes. In conclusion, the Stalnov TNO model certainly proved to be the most promising option among the investigated models. Nonetheless, future studies are required to further investigate and improve the model - particularly for cases featuring realistic flight Reynolds and Mach numbers and very high angles of attack.

Acknowledgments

This project has received funding from the Clean Sky 2 Joint Undertaking under the European Union's Horizon 2020 research and innovation program under grant agreement No CS2-LPAGAM-2014-2015-01.

The authors also thank the NLR (Kylie Knepper) for kindly agreeing to share the experimental data.

References

- [1] Guérin, S., Kissner, C., Seeler, P., Blázquez, R., Laraña, P. C., de Laborderie, H., Lewis, D., Chaitanya, P., Polacsek, C., and Thisse, J., "ACAT1 Benchmark of RANS-Informed Analytical Methods for Fan Broadband Noise Prediction: Part II-Influence of the Acoustic Models," *Acoustics*, Vol. 2, No. 3, 2020, pp. 617–649. <https://doi.org/10.3390/acoustics2030033>.
- [2] Ayton, L. J., Szoke, M., Paruchuri, C. C., Devenport, W. J., and Alexander, W. N., "Trailing-edge serrations: improving theoretical noise reduction models," *27th AIAA/CEAS Aeroacoustics Conference*, 2021. <https://doi.org/10.2514/6.2021-2111>.
- [3] Node-Langlois, T., Wlassow, F., Languille, V., Colin, Y., Caruelle, B., Gill, J. R., Chen, X., Zhang, X., and Parry, A. B., "Prediction of contra-rotating open rotor broadband noise in isolated and installed configurations," *20th AIAA/CEAS Aeroacoustics Conference*, Atlanta, Georgia, USA, 2014. <https://doi.org/10.2514/6.2014-2610>.
- [4] Hu, N., "Empirical model of wall pressure spectra in adverse pressure gradients," *AIAA Journal*, Vol. 56, No. 9, 2018, pp. 3491–3506. <https://doi.org/10.2514/1.J056666>.
- [5] Lee, S., "Empirical wall-pressure spectral modeling for zero and adverse pressure gradient flows," *AIAA Journal*, Vol. 56, No. 5, 2018, pp. 1818–1829. <https://doi.org/10.2514/1.J056528>.
- [6] Hu, N., Reiche, N., and Ewert, R., "Simulation of turbulent boundary layer wall pressure fluctuations via Poisson equation and synthetic turbulence," *Journal of Fluid Mechanics*, Vol. 826, 2017, pp. 421–454. <https://doi.org/10.1017/jfm.2017.448>.

- [7] Hu, N., Reiche, N., and Ewert, R., “Numerical investigation of wall pressure fluctuations for zero and adverse pressure gradient turbulent boundary layers using synthetic anisotropic turbulence,” *23rd AIAA/CEAS Aeroacoustics Conference*, Denver, Colorado, USA, 2017. <https://doi.org/10.2514/6.2017-3200>.
- [8] Rossian, L., Ewert, R., and Delfs, J. W., “Numerical investigation of porous materials for trailing edge noise reduction,” *International Journal of Aeroacoustics*, Vol. 19, No. 6-8, 2020, pp. 347–364. <https://doi.org/10.1177/1475472X20954410>.
- [9] Christophe, J., and Moreau, S., “LES of the trailing-edge flow and noise of a controlled-diffusion airfoil at high angle of attack,” *Proceedings of the Summer Program*, 2008.
- [10] Wang, M., Moreau, S., Iaccarino, G., and Roger, M., “LES prediction of wall-pressure fluctuations and noise of a low-speed airfoil,” *International journal of aeroacoustics*, Vol. 8, No. 3, 2009, pp. 177–197. <https://doi.org/10.1260/2F147547208786940017>.
- [11] Boukharfane, R., Bodart, J., Jacob, M. C., Loly, L., Bridel-Bertomeu, and Nodé-Langlois, T., “Characterization of the pressure fluctuations within a Controlled-Diffusion airfoil boundary layer at large Reynolds numbers,” *25th AIAA/CEAS Aeroacoustics Conference*, Delft, Netherlands, 2019. <https://doi.org/10.2514/6.2019-2722>.
- [12] Choi, H., and Moin, P., “On the space-time characteristics of wall-pressure fluctuations,” *Physics of Fluids A: Fluid Dynamics*, Vol. 2, No. 8, 1990, pp. 1450–1460. <https://doi.org/10.1063/1.857593>.
- [13] Sandberg, R. D., and Sandham, N. D., “Direct numerical simulation of turbulent flow past a trailing edge and the associated noise generation,” *Journal of Fluid Mechanics*, Vol. 596, 2008, pp. 353–385. <https://doi.org/10.1017/S0022112007009561>.
- [14] Moreau, S., Sanjosé, M., Perot, F., and Kim, M.-S., “Direct self-noise simulation of the installed controlled diffusion airfoil,” *17th AIAA/CEAS Aeroacoustics Conference*, Portland, Oregon, USA, 2011. <https://doi.org/10.2514/6.2011-2716>.
- [15] Abe, H., “Reynolds-number dependence of wall-pressure fluctuations in a pressure-induced turbulent separation bubble,” *Journal of Fluid Mechanics*, Vol. 833, 2017, pp. 563–598. <https://doi.org/10.1017/jfm.2017.694>.
- [16] Heisenberg, W., “On the theory of statistical and isotropic turbulence,” *Proceedings of the Royal Society of London. Series A. Mathematical and Physical Sciences*, Vol. 195, No. 1042, 1948, pp. 402–406. <https://doi.org/10.1098/rspa.1948.0127>.
- [17] Batchelor, G. K., *The theory of homogeneous turbulence*, Cambridge university press, 1953.
- [18] Kraichnan, R. H., “Pressure field within homogeneous anisotropic turbulence,” *The Journal of the Acoustical Society of America*, Vol. 28, No. 1, 1956, pp. 64–72. <https://doi.org/10.1121/1.1908224>.
- [19] Panton, R. L., and Linebarger, J. H., “Wall pressure spectra calculations for equilibrium boundary layers,” *Journal of Fluid Mechanics*, 1974, pp. 261–287. <https://doi.org/10.1017/S0022112074001388>.
- [20] Remmler, S., Christophe, J., Anthoine, J., and Moreau, S., “Computation of wall pressure spectra from steady flow data for noise prediction,” *AIAA Journal*, Vol. 48, No. 9, 2010, pp. 1997–2007. <https://doi.org/10.2514/1.J050206>.
- [21] Slama, M., Leblond, C., and Sagaut, P., “A Kriging-based elliptic extended anisotropic model for the turbulent boundary layer wall pressure spectrum,” *Journal of Fluid Mechanics*, Vol. 840, 2018, pp. 25–55. <https://doi.org/10.1017/jfm.2017.810>.
- [22] Grasso, G., Jaiswal, P., Wu, H., Moreau, S., and Roger, M., “Analytical models of the wall-pressure spectrum under a turbulent boundary layer with adverse pressure gradient,” *Journal of Fluid Mechanics*, Vol. 877, 2019, pp. 1007–1062. <https://doi.org/10.1017/jfm.2019.616>.
- [23] Jaiswal, P., Moreau, S., Avallone, F., Ragni, D., and Pröbsting, S., “On the use of two-point velocity correlation in wall-pressure models for turbulent flow past a trailing edge under adverse pressure gradient,” *Physics of Fluids*, Vol. 32, No. 10, 2020, p. 105105. <https://doi.org/10.1063/5.0021121>.
- [24] Parchen, R., “A prediction scheme for trailing edge noise based on detailed boundary layer characteristics,” *Progress report DRAW*, 1998.
- [25] Blake, W. K., *Mechanics of flow-induced sound and vibration, Volume 1 and 2*, Academic press, 2017.
- [26] Kamruzzaman, M., Lutz, T., Würz, W., Shen, W. Z., Zhu, W. J., Hansen, M. O. L., Bertagnolio, F., and Madsen, H. A., “Validations and improvements of airfoil trailing-edge noise prediction models using detailed experimental data,” *Wind Energy*, Vol. 15, No. 1, 2012, pp. 45–61. <https://doi.org/10.1002/we.505>.

- [27] Bertagnolio, F., Fischer, A., and Zhu, W. J., “Tuning of turbulent boundary layer anisotropy for improved surface pressure and trailing-edge noise modeling,” *Journal of Sound and Vibration*, Vol. 333, No. 3, 2014, pp. 991–1010. <https://doi.org/10.1016/j.jsv.2013.10.008>.
- [28] Stalnov, O., Chaitanya, P., and Joseph, P. F., “Towards a non-empirical trailing edge noise prediction model,” *Journal of Sound and Vibration*, Vol. 372, 2016, pp. 50–68. <https://doi.org/10.1016/j.jsv.2015.10.011>.
- [29] Fischer, A., Bertagnolio, F., and Madsen, H. A., “Improvement of TNO type trailing edge noise models,” *European Journal of Mechanics - B/Fluids*, Vol. 61, 2017, pp. 255–262. <https://doi.org/10.1016/j.euromechflu.2016.09.005>.
- [30] Corcos, G. M., “The structure of the turbulent pressure field in boundary-layer flows,” *Journal of Fluid Mechanics*, Vol. 18, No. 3, 1964, pp. 353–378. <https://doi.org/10.1017/S002211206400026X>.
- [31] Chase, D. M., “Modeling the wavevector-frequency spectrum of turbulent boundary layer wall pressure,” *Journal of Sound and Vibration*, Vol. 70, No. 1, 1980, pp. 29–67. [https://doi.org/10.1016/0022-460X\(80\)90553-2](https://doi.org/10.1016/0022-460X(80)90553-2).
- [32] Goody, M., “Empirical spectral model of surface pressure fluctuations,” *AIAA Journal*, Vol. 42, No. 9, 2004, pp. 1788–1794. <https://doi.org/10.2514/1.9433>.
- [33] Rozenberg, Y., Robert, G., and Moreau, S., “Wall-pressure spectral model including the adverse pressure gradient effects,” *AIAA Journal*, Vol. 50, No. 10, 2012, pp. 2168–2179. <https://doi.org/10.2514/1.J051500>.
- [34] Catlett, M. R., Anderson, J. M., Forest, J. B., and Stewart, D. O., “Empirical modeling of pressure spectra in adverse pressure gradient turbulent boundary layers,” *AIAA Journal*, Vol. 54, No. 2, 2016, pp. 569–587. <https://doi.org/10.2514/1.J054375>.
- [35] Willmarth, W. W., and Roos, F. W., “Resolution and structure of the wall pressure field beneath a turbulent boundary layer,” *Journal of Fluid Mechanics*, Vol. 22, No. 1, 1965, pp. 81–94. <https://doi.org/10.1017/S0022112065000599>.
- [36] Amiet, R. K., “Noise due to turbulent flow past a trailing edge,” *Journal of Sound and Vibration*, Vol. 47, No. 3, 1976, pp. 387–393. [https://doi.org/10.1016/0022-460X\(76\)90948-2](https://doi.org/10.1016/0022-460X(76)90948-2).
- [37] Becker, K., Heitkamp, K., and Kügeler, E., “Recent Progress in a Hybrid Grid CFD Solver for Turbomachinery Flows,” *Proc. V European Conference on Computational Fluid Dynamics ECCOMAS CFD 2010*, Lisbon, Portugal, 2010.
- [38] Menter, F. R., “Two-equation eddy-viscosity turbulence models for engineering applications,” *AIAA Journal*, Vol. 32, No. 8, 1994, pp. 1598–1605. URL <https://doi.org/10.2514/3.12149>.
- [39] Weyburne, D., “The Unbounded and Bounded Boundary Layer Models for Flow Along a Wall,” Tech. rep., Air Force Research Laboratory/RYDH Wright-Patterson AFB United States, 2020.
- [40] Moreau, Antoine, “A unified analytical approach for the acoustic conceptual design of fans of modern aero-engines,” Ph.D. thesis, TU Berlin, 2017. <https://doi.org/10.14279/depositonce-5935>.
- [41] Klebanoff, P., “Characteristics of turbulence in a boundary layer with zero pressure gradient,” Tech. rep., National Bureau of Standards Gaithersburg Md, 1955.
- [42] Pope, S. B., *Turbulent flows*, IOP Publishing, 2001. <https://doi.org/10.1088/0957-0233/12/11/705>.
- [43] Donzis, D. A., Sreenivasan, K. R., and Yeung, P., “Scalar dissipation rate and dissipative anomaly in isotropic turbulence,” *Journal of Fluid Mechanics*, Vol. 532, 2005, pp. 199–216. <https://doi.org/10.1017/S0022112005004039>.
- [44] Del Alamo, J. C., and Jimenez, J., “Estimation of turbulent convection velocities and corrections to Taylor’s approximation,” *Journal of Fluid Mechanics*, Vol. 640, 2009, pp. 5–26. <https://doi.org/10.1017/S0022112009991029>.
- [45] Gliebe, P., “Fan broadband self noise prediction model,” *8th AIAA/CEAS Aeroacoustics Conference*, Breckenridge, Colorado, USA, 2002. <https://doi.org/10.2514/6.2002-2490>.
- [46] Efimtsov, B. M., “Characteristics of the field of turbulent wall pressure-fluctuations at large Reynolds-numbers,” *Soviet Physics Acoustics-USSR*, Vol. 28, No. 4, 1982, pp. 289–292.
- [47] Palumbo, D., “Determining correlation and coherence lengths in turbulent boundary layer flight data,” *Journal of Sound and Vibration*, Vol. 331, No. 16, 2012, pp. 3721–3737. <https://doi.org/10.1016/j.jsv.2012.03.015>.

- [48] Kissner, C., Guérin, S., Seeler, P., Billson, M., Chaitanya, P., Carrasco Laraña, P., de Laborderie, H., François, B., Lefarth, K., Lewis, D., Montero Villar, G., and Nodé-Langlois, T., “ACAT1 Benchmark of RANS-Informed Analytical Methods for Fan Broadband Noise Prediction:Part I–Influence of the RANS Simulation,” *Acoustics*, Vol. 2, No. 3, 2020, pp. 539–578. <https://doi.org/10.3390/acoustics2030029>.
- [49] Wilcox, D. C., “Reassessment of the scale-determining equation for advanced turbulence models,” *AIAA journal*, Vol. 26, No. 11, 1988, pp. 1299–1310. <https://doi.org/10.2514/3.10041>.
- [50] Hellsten, A., “New Advanced k-w Turbulence Model for High-Lift Aerodynamics,” *AIAA journal*, Vol. 43, No. 9, 2005, pp. 1857–1869. <https://doi.org/10.2514/1.13754>.
- [51] Wilcox, D. C., *Turbulence modeling for CFD*, Vol. 3, DCW industries, Inc., 2006.
- [52] Cécora, R.-D., Radespiel, R., Eisfeld, B., and Probst, A., “Differential Reynolds-stress modeling for aeronautics,” *AIAA Journal*, Vol. 53, No. 3, 2015, pp. 739–755. <https://doi.org/10.2514/1.J053250>.
- [53] Hanjalić, K., and Jakirlić, S., “Contribution towards the second-moment closure modelling of separating turbulent flows,” *Computers & fluids*, Vol. 27, No. 2, 1998, pp. 137–156. [https://doi.org/10.1016/S0045-7930\(97\)00036-4](https://doi.org/10.1016/S0045-7930(97)00036-4).
- [54] Jakirlić, S., and Hanjalić, K., “A new approach to modelling near-wall turbulence energy and stress dissipation,” *Journal of fluid mechanics*, Vol. 459, 2002, pp. 139–166. <https://doi.org/10.1017/S0022112002007905>.
- [55] Jakirlić, S., “A DNS-based scrutiny of RANS approaches and their potential for predicting turbulent flows,” Postdoctoral lecture qualification, TU Darmstadt, 2004.